Structural, Optical and Electrical Characterization of $KBiFe_2O_5$-ZnO Heterostructure

*Riya Nag, and Abhijit Bera**

Department of Physics, Midnapore College (Autonomous), Raja Bazar Main Rd, 721101

Midnapore, India

Email: abhijit.bera@midnaporecollege.ac.in

ABSTRACT

We formed a binary heterostructure using brownmillerite $KBiFe_2O_5$ and wurtzite ZnO by sol-gel synthesis method. The pure phase of the individual materials and the composite phase of heterostructure were characterized by X-ray diffraction spectra and FESEM morphologies. Optical absorbance spectroscopy was employed to estimate the optical band gap of individual materials and the heterostructure. While $KBiFe_2O_5$ absorbs most of the visible region, ZnO nanoparticles are used to fabricate staggered type-II band alignment in the heterostructure. The electrical and dielectric properties of the materials were obtained by fabricating thin film devices and measuring current-voltage characteristics and impedance spectroscopy, respectively. The double logarithm plot of the I-V data reveals three distinct regions which explained the charge transport mechanism through the devices. However, the electrical properties reveal lower resistance and better charge transport properties in heterostructures compared to individual materials which are essential for evolving optoelectronic applications.

KEYWORDS: $KBiFe_2O_5$-ZnO heterostructure, XRD-analysis, optical characterization, current-voltage characteristics, impedance spectroscopy

INTRODUCTION

Recently multiferroics are considered very exciting materials for their multifunctional properties such as magnetic, dielectric, photovoltaic, photocatalytic, ferroelectric etc. Due to these multifaceted characteristics, they act as a potential candidate for the fabrication of the new-

generation technological device.[1-4] One such discovery is $BiFeO_3$, a regular perovskite that possesses multiferroic properties and a moderate band gap (~2.6 eV) due to the effect of magnetically ordered e-e interaction.[5-9] But the main drawback of $BiFeO_3$ in the photovoltaic application is their band gap which is not lie in the visible range. Due to this deficiency, there is a need for improvement in the $BiFeO_3$ perovskite structure for welcoming an alternative material. From this standpoint, brownmillerite structured $KBiFe_2O_5$ ($A_2B_2O_5$) is a freshly discovered material with a low band gap of ~1.6 eV, admissible for good photovoltaic performance.[10] The deduction in band gap value is well described by a more ordered arrangement of corner-sharing FeO_4 tetrahedrons as well as the short metal-oxide (Fe-O) bond length of $KBiFe_2O_5$. The corner-sharing FeO_6 octahedrons of $BiFeO_3$ lose their magnetic and dielectric behaviour at higher temperatures but high covalence in FeO_4 tetrahedrons express $KBiFe_2O_5$ as a potential brownmillerite material.[11-13] Therefore it has been considered a lead-free and cost-effective photoactive material. But still, there is an inadequacy in light absorbance capacity and photogenerated e-h pair stability. Heterostructure formation, metal doping, and grain size variation are the solution to this specific issue.[14] The best way to overcome this problem is heterojunction formation by other semiconductors.[15-16] $KBiFe_2O_5$ is an intrinsic material so it can be approached for heterostructure formation with suitable n-type or p-type materials. ZnO (E_g ~3.1 eV) is a traditional n-type semiconducting material and acts as a promising candidate for their high light absorbance capacity.[17-19]

In this work, we have synthesized $KBiFe_2O_5$ brownmillerite using the sol-gel method. After that $KBiFe_2O_5$-ZnO heterostructure was formed by loading ZnO nanoparticles on the surface of $KBiFe_2O_5$ to create a type-II heterojunction. The light absorbance capacity as well as the lifetime of photoinduced e-h pair created in the heterojunction is more upgraded due to ZnO nanoparticles insertion. As a consequence, $KBiFe_2O_5$-ZnO act as better charge transport and has low resistance properties compared to the bare $KBiFe_2O_5$.

EXPERIMENTAL SECTION

Materials

The reagents, bismuth nitrate pentahydrate (98.5% pure), iron nitrate nonahydrate (98% pure), potassium nitrate (98% pure), potassium hydroxide (84% pure), zinc acetate dihydrate (98% pure),

ethylene glycol (99% pure) were used for $KBiFe_2O_5$ formation with no other additional purification.

Synthesis of $KBiFe_2O_5$ Nanoparticles

In this study, $KBiFe_2O_5$ nanomaterials were synthesized by a sol-gel method. 2.5 mmol Potassium nitrate (KNO_3), 2.5 mmol Bismuth (III) nitrate pentahydrate ($Bi(NO_3)_3 \cdot 5H_2O$) and 5 mmol iron(III) nitrate nonahydrate ($Fe(NO_3)_3 \cdot 9H_2O$)were added to 12 ml ethylene glycol as precursors. All the contents were magnetically agitated for 1 hour to get a uniform and transparent dark red coloured solution. The oven temperature was maintained at 80ºC for a dark yellow gel formation. The stirring conditions were continued for the evaporation of the entire liquid and this yellow gel was dried at 100ºC for another 30 min. Then the oven temperature was further raised to 350ºC at a rate of 5ºC/min to obtain a rust colour sample and the synthesized materials were annealed at 645ºC for 30 min. The dark brown sample was grounded by mortar to obtain a dark brown fine powdered sample. Then the obtained sample was washed with alcohol and distilled water and the dried sample was kept in a glass jar for further experiment.

Synthesis of ZnO Nanoparticles

We have pursued a route of previous literature for the fabrication of ZnO nanoparticles.[20] We made ready two different suspensions of zinc acetate dihydrate ($Zn(CH_3COO)_2.2H_2O$) and potassium hydroxide (KOH) in methanol. Two separate precursors mixture were prepared by adding 13.4 mmol zinc acetate dihydrate to 63 ml methanol and 23 mmol potassium hydroxide to 33 ml methanol in a beaker. Two beakers were kept in an ultrasonication bath for 30 min to get a uniform suspension. Zinc acetate solution was placed on a magnetic stirrer and the potassium hydroxide solution was added dropwise (30 min) to the solution at a constant temperature of 60ºC. A white precipitate gradually appeared and change the transparent solution into a white precipitated solution. The precipitated solution was magnetically agitated for another 1 hour under the same environments to complete the reaction. To collect the nanoparticles the solution was centrifuged twice and dried with a vacuum dryer. The sample was grounded by mortar to get a white colour fine powdered sample.

Formation of the Heterostructure

To develop the core-shell $KBiFe_2O_5$-ZnO heterostructure three different solutions were assembled in methanol solvent. The 1st solution was prepared by adding 0.21 gm $KBiFe_2O_5$ to 12.5 ml methanol, the 2nd solution was prepared by adding 0.544 gm zinc acetate dihydrate to 7.5 ml

methanol, for the 3rd solution was prepared by adding 0.28 gm KOH to 5 ml methanol. The 3 beakers were placed in an ultrasonication bath for 30 min followed by 30 min of magnetic stirring to obtain a homogeneous and uniform solution. The 1st solution was magnetically stirred at 500 rpm, then the 2nd and 3rd solutions were added slowly and simultaneously (30 min) with the 1st one. And this final solution was allowed to stir for another 30 min. The synthesised solution was washed twice by centrifugation process and dried with a vacuum dryer. The final sample was calcinated at 100°C for 30 min and the powder was stored in a glass jar for further use.

Characterization of the Material

The as-prepared materials were studied by optical X-ray diffraction (XRD) using a Rigaku Miniflex 600 powder diffractometer, scanning electron microscopy (FE-SEM) using a Zeiss FESEM, surface morphology using a Park XE7 AFM (Park Systems Corp., South Korea). The morphological and thickness study was done by non-contact mode AFM (tip radius of 20 nm approx.) under the ambient condition at a scan rate of 0.5 Hz.

Device fabrication

The device was fabricated on indium tin oxide (ITO)-coated glass substrates, used as a bottom electrode having a surface resistance of (10-15) Ω/cm^2. The ITO substrates were cleaned following the usual protocol. To fabricate the devices, a high concentration (60 mg/ml) of dispersed methanolic solution of $KBiFe_2O_5$ and $KBiFe_2O_5$-ZnO nanoparticles was prepared by the sonication and filtration method. The solutions were then drop-casted onto the clean ITO substrates and left for 5 minutes to evaporate the solvents and form a thick film on the substrate. After that, the film was annealed at 180 °C for 30 min in an oxygen environment. This process yields a film thickness of (0.8 ± 0.1) μm, determined from the scratch profile in AFM. For the top electrode, we used concentrated silver paste solution in the form of a 4 mm diameter circular spot. This completed the device fabrication process with the active area of each cell being ~ 6 mm^2.

Characterization of the Devices

Current-voltage (I−V) characteristics under dark conditions were recorded with a manually controlled electrometer. The impedance spectroscopy was measured by HIOKI IM3536 LCR Meter.

RESULTS AND DISCUSSIONS

$KBiFe_2O_5$ nanoparticle was prepared by sol-gel method using ethylene glycol as a solvent and for the formation of $KBiFe_2O_5$-ZnO heterostructure, we have followed the reported literature. Figure

1(a-c) shows the crystallinity of synthesized materials, which are analyzed by the room-temperature X-ray diffractometer. The XRD pattern of $KBiFe_2O_5$ calcinated at 645°C shown in figure 1(a) confirms the pure monoclinic $KBiFe_2O_5$ crystal phase as all the peaks matched well with the reported work. The unit cell parameters of a single-phase monoclinic structure are a= 7.8932 Å, b=5.9734 Å, c=5.7256 Å and α=γ=90° and β= 94.46° with the P2/c space group.[21] Figure 1(b) represents the crystalline structure of ZnO nanoparticles with the strong diffraction peaks at 31.83°, 34.42° and 36.27° corresponding to the (100), (002) and (101) diffraction planes respectively. The XRD pattern presented in Figure 1(c) exhibited all the sharp peaks of bare $KBiFe_2O_5$ and ZnO which confirm the formation of $KBiFe_2O_5$-ZnO heterostructure. The topographical information of synthesized $KBiFe_2O_5$ is investigated by FESEM shown in Figure 1(d) which represents single-phase well-ordered grain distribution. A regular arrangement of ZnO nanoparticles is shown in Figure 1(e). Figure 1(f) reveals the enlarged grain size of $KBiFe_2O_5$-ZnO heterostructure with larger porosity which can support it as an active photovoltaic material.

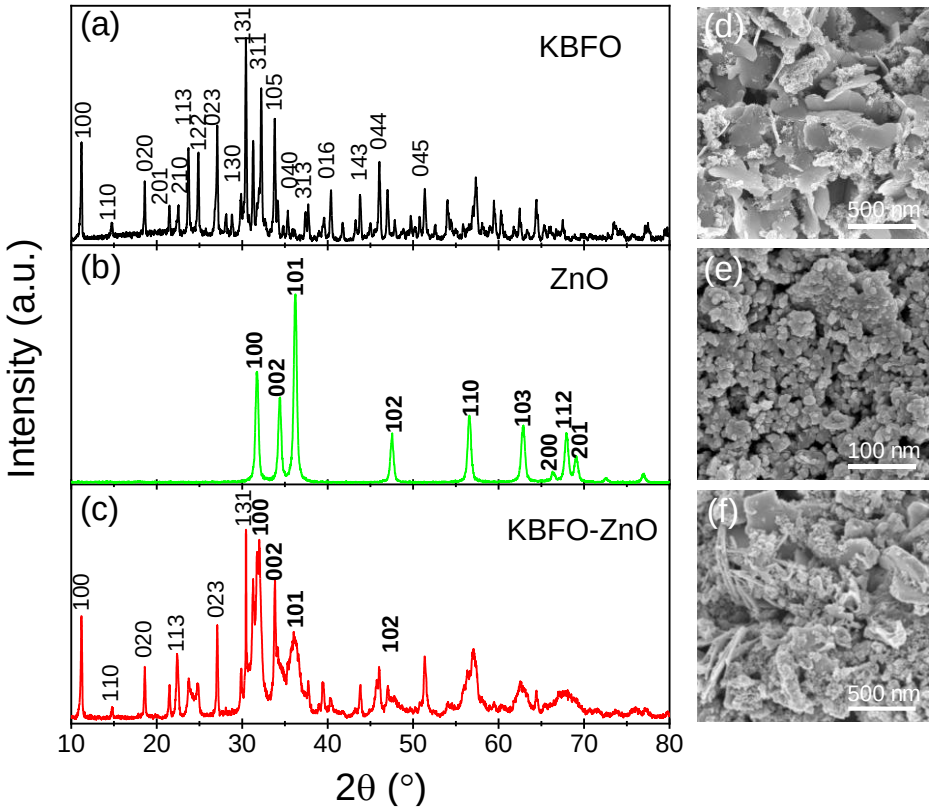

Figure 1. Structural properties of $KBiFe_2O_5$-ZnO heterostructures: (a-c) XRD spectra and (d-f) corresponding FESEM morphology of $KBiFe_2O_5$ (a,d), ZnO nanoparticle (b,e), and $KBiFe_2O_5$-ZnO heterostructure (c,f). Some lattice planes are marked in the inset.

To investigate the optical band gap of the individual sample of $KBiFe_2O_5$, ZnO, and $KBiFe_2O_5$-ZnO heterostructure we have studied the UV-Visible spectroscopy of those samples shown in figure 2(a). The as-synthesized $KBiFe_2O_5$ exhibited optical absorption in a broad region of the UV-Visible range with maximum absorption at 430 nm. The optical band gap of $KBiFe_2O_5$, ZnO, and $KBiFe_2O_5$-ZnO was estimated as 1.78 eV and 3.07 eV and 2.28 eV respectively using the Tauc relation corresponding to the optical absorption spectra reveals in figure 2(b).[11, 17] The evaluated values of the band gap of $KBiFe_2O_5$ and ZnO are closely reconcilable with the previous literature. The band gap value of $KBiFe_2O_5$-ZnO core-shell has a perfect spectral match with the visible light spectrum which leads to acting as a superior material for photovoltaic applications.

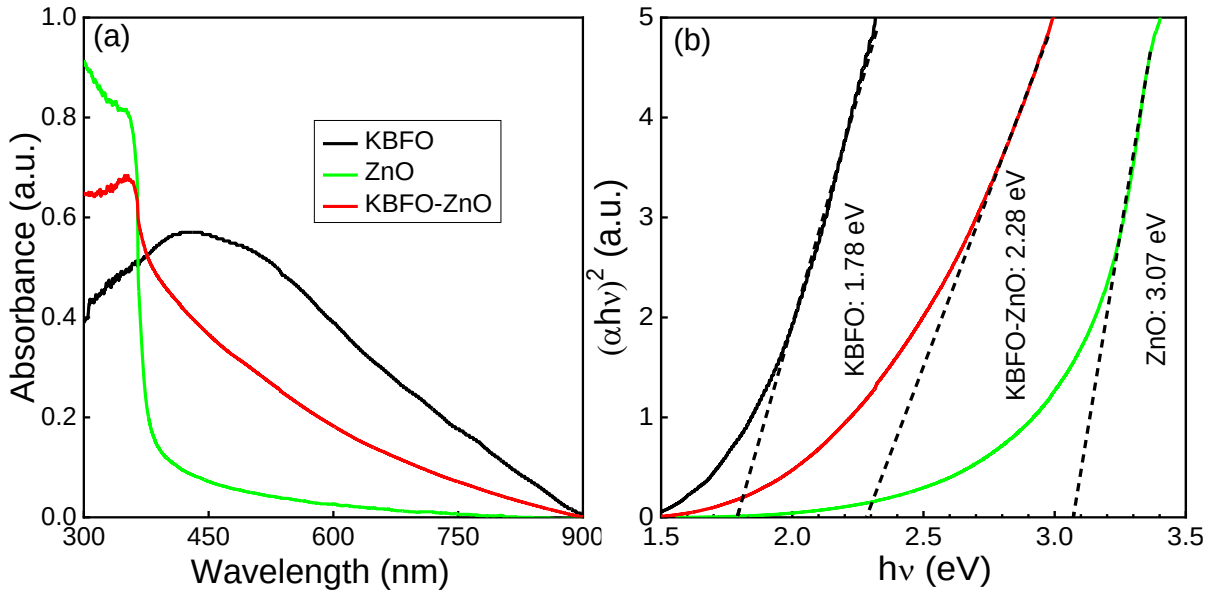

Figure 2. Optical characteristics of heterostructure: (a) optical absorption spectrum of $KBiFe_2O_5$ (open circle), ZnO (asterisk) and heterostructure $KBiFe_2O_5$-ZnO (filled circle) in methanol solution. (b) Plot of $(\alpha h\nu)^2$ versus energy, with the broken line being used to determine the bandgap of the materials. The estimated optical band gap of individual materials and the heterostructure are presented in the inset.

The morphological study of prepared $KBiFe_2O_5$ and ZnO thin film, presented in Figure 3(a) and (b) is analyzed by non-contact mode AFM. Figure 3(c) shows the topography and corresponding scratch profile of the $KBiFe_2O_5$-ZnO thin film. The scratch profile of $KBiFe_2O_5$-ZnO reveals a thickness of 831 nm and roughness of the thin film depicted in the inset of figure 3(c). The film

morphology of the $KBiFe_2O_5$-ZnO heterostructure exhibits a flat and continuous surface which can act as an efficient current-voltage (I-V) device by reducing the leakage current.

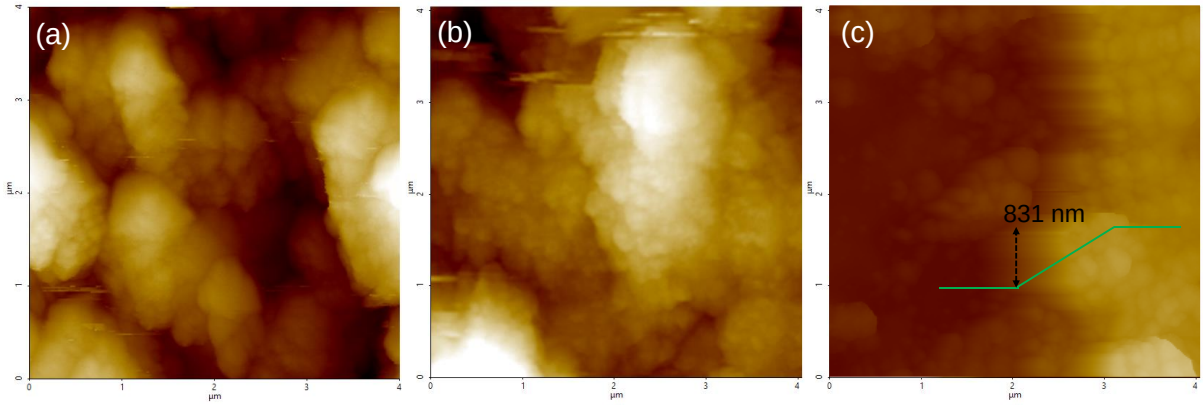

Figure 3. Surface morphology and scratch profile of thin films: (a-b) AFM morphology of $KBiFe_2O_5$ (a) and ZnO (b) thin film. (c) Morphology and corresponding scratch profile of $KBiFe_2O_5$-ZnO heterostructure.

The I-V characteristics of both $KBiFe_2O_5$ and $KBiFe_2O_5$-ZnO in Figure 4a with a device structure of ITO/ Active layer/Ag indicate a rectifying nature with a high current in the forward directions and a constant low saturation current in the reverse direction. This non-linear nature arises mainly due to the Schottky junction formation between the ITO electrode and the semiconductor of the active layer. The current magnitude is considerably increased in the $KBiFe_2O_5$-ZnO device compared to the bare $KBiFe_2O_5$ due to the incorporation of high electron transport ZnO nanoparticles and the formation of type-II band alignment inside the active layer.

The charge transport mechanism is also explained by plotting the double logarithmic J–V characteristics of the devices. In the plot of Figure 4d, we mainly identified three regions with different slopes, following the power-law relationship $I \propto V^m$, where m corresponds to the slope of the curve. In the low-voltage region (region I), a slope of 1.5 and 1.2 was determined for $KBiFe_2O_5$ and $KBiFe_2O_5$-ZnO devices respectively. Furthermore, in the intermediate (region II) and high-voltage (region III) portions, the slopes were found to be 2.2 and 1.4, and 1.5 and 2.7, respectively. These different slopes signify a space charge-limited conduction (SCLC) mechanism assisted by the exponential distribution of traps located inside the active material. The regions I, II, and III is therefore said to be trap-limited SCLC, trap-filled limited, and trap-free SCLC,

respectively.[22] In region I, the injected carriers are fewer in number, and the traps inside the material begin to fill up. After all the traps are filled at the intermediate bias (region II), the increased number of electrons due to the high bias in region III forms the space charge. The conduction then essentially becomes a space charge limited in this region. In the $KBiFe_2O_5$-ZnO device, the slope of the intermediate region was considerably higher than the bare $KBiFe_2O_5$ device due to the presence of ZnO trap states which took a broader range of voltage region to fill up.

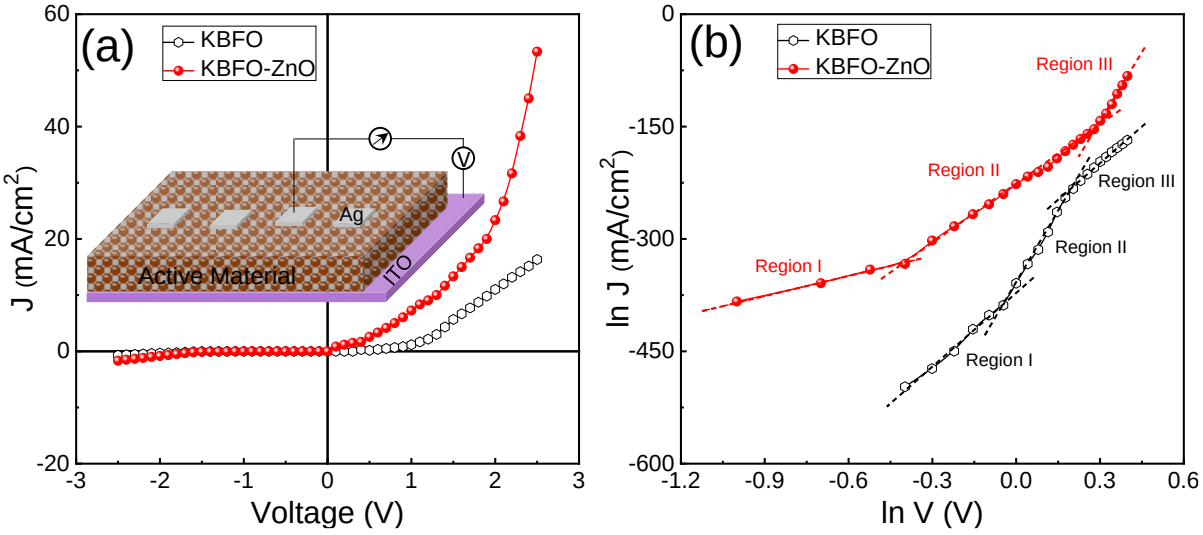

Figure 4. Current-voltage characteristics of the heterostructure: (a) J-V characteristics of the device with $KBiFe_2O_5$ active layer (open circle) and $KBiFe_2O_5$-ZnO heterostructures (filled circle) under dark conditions. A schematic representation of the device (inset of a). (b) Double logarithmic J–V plot of the same device.

The impedance spectroscopy of the devices was carried out using an LCR meter in the frequency range 100 Hz–1 MHz at 500 mV bias voltage dark ambient conditions. The equivalent circuit for the fitted spectra shown in the inset of Figure 5a consists of circuit elements R_1, R_2, and C_1. Here, R_1 is the series resistance corresponding to the resulting resistance occurring from the connecting wires, electrode, and substrate, R_2 is the charge transfer resistance (R_{ct}), and C_p refers to the double-layer capacitance. The parameters of the device were measured by Nyquist plot. From the plot, the high-frequency region gets mainly dominated by a semi-circular arc representing the resistance to the charge transfer process inside the device. The diameter of the semicircle is significantly reduced after the incorporation of ZnO nanoparticles in the $KBiFe_2O_5$. This explains the higher

current magnitude in the $KBiFe_2O_5$-ZnO-based device. Additionally, the capacitance value is also reduced in the composite device due to the heterostructure formation. The parameters of the devices with different thickness films are presented in the inset of Figure 5b. Thus, the $KBiFe_2O_5$-ZnO composite reveals better charge transport properties which are essential for the fabrication of optoelectronic applications.

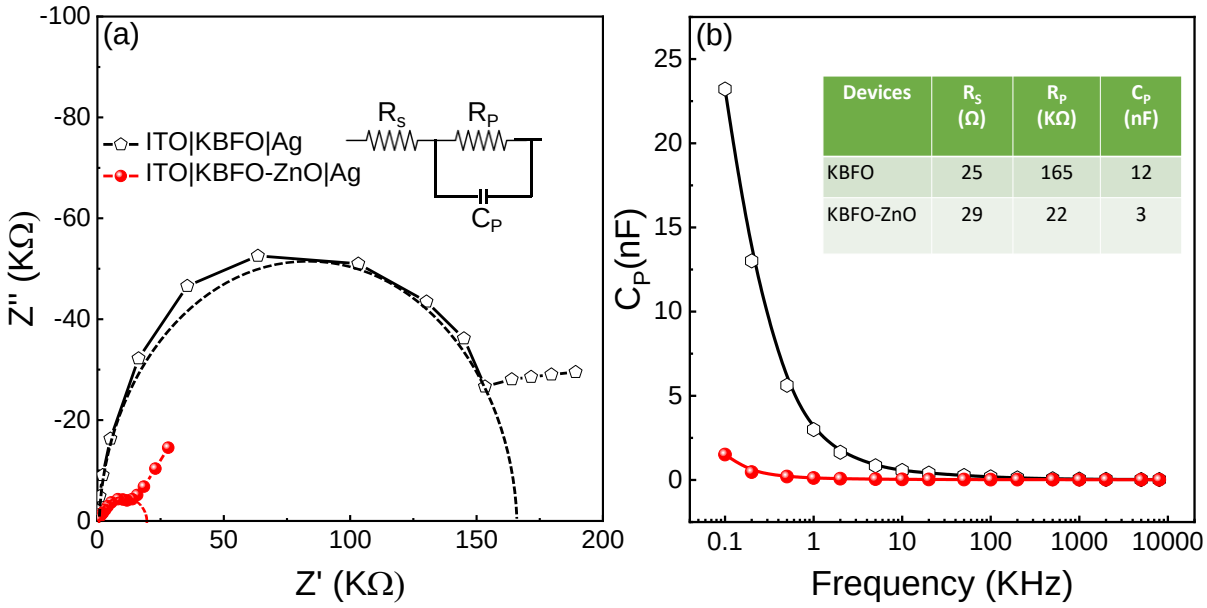

Figure 5. Impedance spectroscopy of the device: (a) Nyquist plot of the ITO-Active layer-Ag device under dark conditions. An equivalent circuit of the device (inset). (b) Frequency-dependent capacitance plot of the device.

CONCLUSIONS

In conclusion, we have formed a binary heterostructure using a brownmillerite $KBiFe_2O_5$ and a ZnO nanoparticle and characterize their electrical and dielectric properties. The pure phase of brownmillerite $KBiFe_2O_5$ and the wurtzite phase of ZnO is confirmed by XRD spectroscopy. The presence of both materials in the heterostructure was also confirmed by XRD spectra and FESEM morphologies. The optical property was investigated through UV-Vis absorbance spectroscopy. While $KBiFe_2O_5$ absorbs most of the visible region, ZnO absorbs only in the UV region which exhibits an optical band gap of 1.8 eV and 3.1 eV, respectively. As a result, the heterostructure reveals an intermediate band gap of 2.3 eV which is effective for the fabrication of optoelectronic devices. The dark I-V characteristics reveal a rectifying characteristic when forming a Schottky device on the ITO substrate. The current density of the $KBiFe_2O_5$-ZnO device reveals 2.5 times

higher than the bare $KBiFe_2O_5$ device. The J-V plot and the dielectric measurements reveal better charge transport and low capacitance properties in the $KBiFe_2O_5$-ZnO device solely due to the formation of the heterostructure. Thus, the formation of heterostructure using a low band gap $KBiFe_2O_5$ with an electron transport ZnO nanoparticle can be used as an efficient optoelectronic material.

ACKNOWLEDGMENT

This work was supported by the SERB, India grant under file no. EEQ/2020/000156. RN acknowledges SERB for funding the project fellowship.

REFERENCES

[1] H. Zou, X. Hui, X. Wang, D. Peng, J. Li, Y. Li, X. Yao, Luminescent, dielectric, and ferroelectric properties of Pr doped $Bi_7Ti_4NbO_{21}$ multifunctional ceramics, J. Appl. Phys. 114 (2013) 223103.

[2] J. H. Im, I. H. Jang, N. Pellet, M. Grätzel, N. G. Park, Growth of $CH_3NH_3PbI_3$ cuboids with controlled size for high-efficiency perovskite solar cells, Nat. Nanotechnol. 9 (2014) 927-932.

[3] W. Zhang, G. E. Eperon, H. J. Snaith, Metal halide perovskites for energy applications, Nat. Energy 1 (2016) 16048.

[4] J. Chen, X. Xing, A. Watson, W. Wang, R. Yu, J. Deng, L. Yan, C. Sun, X. Chen, Rapid synthesis of multiferroic BiFeO3 single-crystalline nanostructures, Chem. Mater. 19 (2007) 3598-3600.

[5] T. Choi, S. Lee, Y. J. Choi, V. Kiryukhin, S.-W. Cheong, Switchable ferroelectric diode and photovoltaic effect in $BiFeO_3$, Science 324 (2009) 63-66.

[6] H. Wu, P. Xue, Y. Lu, X. Zhu, Microstructural, optical and magnetic characterizations of $BiFeO_3$ multiferroic nanoparticles synthesized via a sol-gel process, J. Alloys Compd. 731 (2018) 471-477.

[7] A. K. Sinha, B. Bhushan, Jagannath, R. K. Sharma, S. Sen, B. P. Mandal, S. S. Meena, P. Bhatt, C. L. Prajapat, A. Priyam, S. K. Mishra, S. C. Gadkari, Enhanced dielectric, magnetic and optical properties of Cr-doped $BiFeO_3$ multiferroic nanoparticles synthesized by sol-gel route, Results Phys. 13 (2019) 102299.

[8] S. M. Selbach, T. Tybell, M-A. Einarsrud, T. Grande, Size-Dependent properties of multiferroic $BiFeO_3$ nanoparticles, Chem. Mater. 19 (2007) 6478-6484.

[9] T.-J. Park, G. C. Papaefthymiou, A. J. Viescas, A. R. Moodenbaugh, S. S. Wong, Size-dependent magnetic properties of single-crystalline multiferroic $BiFeO_3$ nanoparticles, Nano Lett. 7 (2007) 766-772.

[10] G. Zhang, H. Wu, G. Li, Q. Huang, C. Yang, F. Huang, F. Liao, J. Lin, New high Tc multiferroics $KBiFe_2O_5$ with narrow band gap and promising photovoltaic effect, Sci. Rep. 3 (2013) 1723.

[11] D. S. Vavilapalli, K. Srikanti, R. Mannam, B. Tiwari, K. K. Mohan, M. S. Ramachandra Rao, S. Singh, Photoactive brownmillerite multiferroic $KBiFe_2O_5$ and its potential application in sunlight-driven photocatalysis, ACS Omega 13 (2018) 16643-16650.

[12] R. Rai, A. George, V. S. Muthukumar, K. B. R. Varma, R. Philip, M. Molli, Investigation of nonlinear optical and photocatalytic properties of sol-gel derived $KBiFe_2O_5$, J. Mater. Sci.: Mater. Electron. 30 (2019) 11451-11457.

[13] D. S. Vavilapalli, A. A. Melvin, S. Kavita, A. K. Yadav, S. N. Jha, D. Bhattacharyya, S. Ch. Sarma, S. C. Peter, M. S. Ramachandra Rao, S. Singha, Multifunctional brownmillerite $KBiFe_2O_5$: Structural, magneto-dielectric, optical, photoelectrochemical studies and enhanced photocatalytic activity over perovskite $BiFeO_3$, Sol. Energy Mater. Sol. Cells 200 (2019) 109940.

[14] R. Rai, M. Molli, Magnetic, optical and photocatalytic properties of yttrium doped $KBiFe_2O_5$, Appl. Phys. A Mater. Sci. Process 125 (2019) 878.

[15] K. Afroz, Md Moniruddin, N. Bakranov, S. Kudaibergenov, N. Nuraje, A heterojunction strategy to improve the visible light sensitive water splitting performance of photocatalytic materials, J. Mater. Chem. A 6 (2018) 21696.

[16] Sonu, V. Dutta, S. Sharma, P. Raizada, A. Hosseini-Bandegharaei, V. K. Gupta, P. Singh, Review on augmentation in photocatalytic activity of $CoFe_2O_4$ via heterojunction formation for photocatalysis of organic pollutants in water, J. Saudi Chem. Soc. 23 (2019) 1119-1136.

[17] S. E. Ahn, J. S. Lee, H. Kim, S. Kim, B. H. Kang, K. H. Kim, G. T. Kim, Photoresponse of sol-gel synthesized ZnO nanorod, Appl Phys Lett 84 (2004) 5022.

[18] H. Razavi-Khosroshahi, K. Edalati, J. Wu, Y. Nakashima, M. Arita, Y. Ikoma, M. Sadakiyo, Y. Inagaki, A. Staykov, M. Yamauchi, Z. Horita, M. Fuji, High-pressure zinc oxide phase as

visible-light-active photocatalyst with a narrow band gap, J. Mater. Chem. A 5 (2017) 20298-20303.

[19] E. Karamian, S. Sharifnia, Enhanced visible light photocatalytic activity of $BiFeO_3$-ZnO p-n heterojunction for CO_2 reduction, Mater. Sci. Eng 238-239 (2018) 142-148.

[20] S. Chatterjee, A. Bera, A. J. Pal, p-i-n heterojunctions with $BiFeO_3$ perovskite nanoparticles and p- and n-type oxides: photovoltaic properties, ACS Appl. Mater. Interfaces 6 (2014) 20479-20486.

[21] R. Nag, S. Paul, A. Bera, A Type-II heterostructure with a $KBiFe_2O_5$ brownmillerite core and a ZnO nanoparticle shell for enhanced optoelectronic performance, ChemistrySelect 7 (2022) e202202802.

[22] M. Nayak, R. Nag, A. Bera, A. J. Akhtar, S. K. Saha Schottky analysis of formamidinium lead halide perovskite nanocrystals' devices with enhanced stability, Appl. Nanosci. 12 (2022) 2671–2681.